

# Wavelet Frame-Based Fuzzy C-Means Clustering for Segmenting Images on Graphs

Cong Wang, Witold Pedrycz<sup>ID</sup>, Fellow, IEEE, JianBin Yang<sup>ID</sup>, MengChu Zhou<sup>ID</sup>, Fellow, IEEE,  
and ZhiWu Li<sup>ID</sup>, Fellow, IEEE

**Abstract**—In recent years, image processing in a Euclidean domain has been well studied. Practical problems in computer vision and geometric modeling involve image data defined in irregular domains, which can be modeled by huge graphs. In this paper, a wavelet frame-based fuzzy *C*-means (FCM) algorithm for segmenting images on graphs is presented. To enhance its robustness, images on graphs are first filtered by using spatial information. Since a real image usually exhibits sparse approximation under a tight wavelet frame system, feature spaces of images on graphs can be obtained. Combining the original and filtered feature sets, this paper uses the FCM algorithm for segmentation of images on graphs contaminated by noise of different intensities. Finally, some supporting numerical experiments and comparison with other FCM-related algorithms are provided. Experimental results reported for synthetic and real images on graphs demonstrate that the proposed algorithm is effective and efficient, and has a better ability for segmentation of images on graphs than other improved FCM algorithms existing in the literature. The approach can effectively remove noise and retain feature details of images on graphs. It offers a new avenue for segmenting images in irregular domains.

**Index Terms**—Fuzzy *C*-means (FCM) algorithm, image on graphs, image segmentation, spatial information, tight wavelet frames.

Manuscript received January 12, 2019; revised April 14, 2019; accepted June 3, 2019. Date of publication July 10, 2019; date of current version August 18, 2020. This work was supported in part by the Fundamental Research Funds for the Central Universities and the Innovation Fund of Xidian University, in part by the National Natural Science Foundation of China under Grant 11771120, Grant 61472295, and Grant 61672400, in part by the Recruitment Program of Global Experts, and in part by the Science and Technology Development Fund, MSAR, under Grant 0012/2019/A3. This paper was recommended by Associate Editor A. F. Skarmeta Gomez. (*Corresponding authors:* MengChu Zhou; ZhiWu Li.)

C. Wang is with the School of Electro-Mechanical Engineering, Xidian University, Xi'an 710071, China (e-mail: wangc0705@stu.xidian.edu.cn).

W. Pedrycz is with the Department of Electrical and Computer Engineering, University of Alberta, Edmonton, AB T6R 2V4, Canada, also with the School of Electro-Mechanical Engineering, Xidian University, Xi'an 710071, China, and also with the Faculty of Engineering, King Abdulaziz University, Jeddah 21589, Saudi Arabia (e-mail: wpedrycz@ualberta.ca).

J. Yang is with the College of Science, Hohai University, Nanjing 211100, China (e-mail: jbyang@hhu.edu.cn).

M. Zhou is with the Institute of Systems Engineering, Macau University of Science and Technology, Macau 999078, China, and also with the Helen and John C. Hartmann Department of Electrical and Computer Engineering, New Jersey Institute of Technology, Newark, NJ 07102 USA (e-mail: zhou@njit.edu).

Z. Li is with the Institute of Systems Engineering, Macau University of Science and Technology, Macau 999078, China, and also with the School of Electro-Mechanical Engineering, Xidian University, Xi'an 710071, China (e-mail: zhwl@xidian.edu.cn).

Color versions of one or more of the figures in this paper are available online at <http://ieeexplore.ieee.org>.

Digital Object Identifier 10.1109/TCYB.2019.2921779

## I. INTRODUCTION

IN RECENT years, image segmentation has been playing an increasing important role in computer vision and geometric modeling. It aims to divide an image into a number of nonoverlapping areas that have the same characteristics, such as gray level, color, texture, and tone. Over the past two decades, image segmentation in a Euclidean space has received much attention, resulting in a series of achievements [1]–[4], [11], [12], [22], [24], [30]. However, as graphs can be flexibly represented in either Euclidean domain or irregular domains [8], [43], researchers have recently started to analyze and manipulate structured data that are composed of sampled real-valued functions defined on graphs [16], [42], [43], [45]. In practical applications, in general, graphs can be modeled as a certain discretization or random sample from some Riemannian manifolds [39]. Many structured datasets, like point clouds and 3-D mesh surfaces, can be considered as scalar functions defined on vertices of graphs. Under such circumstances, it becomes an important topic to design efficient computing methods for addressing image processing problems defined on graphs.

Many efforts have been made to solve image processing problems defined on graphs [16], [34], [43], [45]. For instance, Niyobuhungiro and Setterqvist [34] established an analog of the Rudin–Osher–Fatemi (ROF) model [37] defined on graphs and proposed a new algorithm to solve this model. Dong [16] presented a fast discrete tight wavelet frame transform in a graph domain, which is applied to many practical problems, such as graph data denoising and semisupervised clustering. More recently, Wang and Yang [43] introduced a variation method with tight wavelet frames to remove Poisson noise (PN) in images on graphs.

Clustering has been successfully applied to image segmentation in a Euclidean space. In the past, a large number of clustering-based algorithms realized for image segmentation were presented [20], [22], [24]. Many traditional clustering-based methods, like density-based methods, hierarchical methods, and the *K*-means algorithm, assign pixels exclusively to a single cluster. Differing them, a fuzzy *C*-means (FCM) algorithm allows pixels to have varying degrees of membership to multiple clusters. Thus, it is practically compelling with a considerable number of advantages.

The main contribution of this paper is a wavelet frame-based FCM algorithm for segmenting images on graphs, so as to improve the effectiveness of the original FCM algorithm. Its overview is shown in Fig. 1. To enhance the robustness

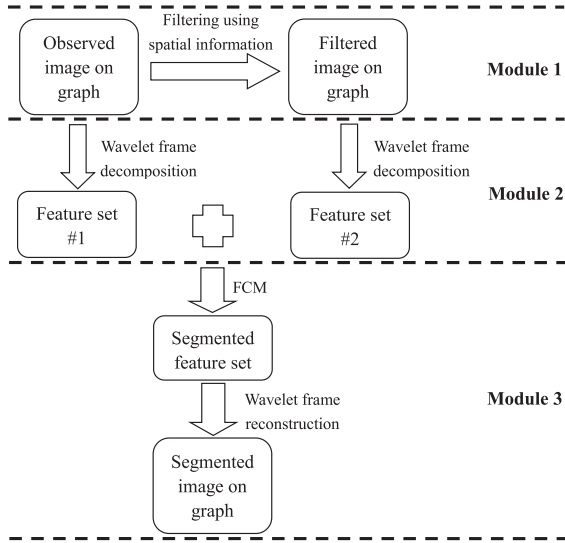


Fig. 1. Wavelet frame-based FCM algorithm for segmenting images on graphs: an overview.

of FCM, observed images on graphs are first filtered by using available spatial information. Then, a tight wavelet frame system is used to obtain high and low frequency information of the original images and filtered images on graphs, thus forming feature spaces of images. Taking these spaces as data patterning, FCM is utilized to segment images on graphs. Finally, the segmented images are reconstructed by the wavelet frame transform on graphs.

The essence of the underlying idea that the original space (time domain) is transformed to a new feature space (frequency domain) by a nonlinear mapping (wavelet frame transform). The new feature space has an enhanced discriminatory capability to analyze and manipulate image data on graphs. Traditionally, image pixel values are considered to be data of FCM. In contrast, taking the nature of tight wavelet frames on graphs as a starting point, this paper utilizes tight wavelet frames to decompose image pixels into feature spaces, that is, high and low frequency information, which means that underlying image features and noise can be found. We anticipate that FCM with feature spaces can not only remove noise but also segment images on graphs more accurately. In other words, the proposed algorithm is actually a kernel-based FCM algorithm [9], [23]–[25], [38], [47]. The tight wavelet frames can be regarded as a kernel function. In this paper, we develop this suitable kernel-based FCM algorithm, which is designed for the problems of segmenting images on graphs.

This paper is organized as follows. Section II reviews different image segmentation techniques, especially conceptual developments and application studies of FCM, and makes some comments upon the state-of-the-art. Section III briefly introduces the wavelet frame transform on graphs and FCM. Section IV formulates the proposed algorithm in detail. In Section V, experimental results on synthetic and real images on graphs are provided. The conclusions are drawn in Section VI.

## II. LITERATURE REVIEW

In this section, we briefly review different image segmentation techniques. Image segmentation techniques are broadly classified into four categories, *viz.*, intensity thresholding technique [41], edge-based approach [35], region-based approach [21], and classification-based approach [44], [47].

In intensity thresholding techniques [41], the adjacent pixels belong to the same class, which is based on the determination of a certain threshold level of an image. Once intensity values of pixels exceed the threshold value, they are assigned to one segment and the remaining to the other. Due to the lack of optimal threshold, this technique could fail. The edge-based approaches [35] are generally related to edge detection. By using some edge detection algorithms, interrupted contour lines around an object of interest are first generated. Based on some similarity criteria, these lines are added to detect the object or region of interest. The main drawback of the edge-based approaches is computationally expensive post-processing for the acquisition of hole free representation of the objects. The region-based approaches [21] develop the thresholding techniques by combining an intensity similarity measure to obtain connectivity of pixels. A seed point (pixel) is first selected for each region. Based on homogeneity criteria, pixels in the neighborhood are added to the regions, which results in connected regions. Different regions represent different visual features of images. However, they are sensitive to noise.

The classification-based approaches [44], [47] have been broadly used in image segmentation. Among these approaches, the FCM algorithm is more effective than others with considerable amount of benefits. In 1973, Dunn [19] proposed the FCM algorithm. In 1981, it was further improved by Bezdek [6]. Over the past three decades, researchers have realized a series of improvements with respect to its conceptual developments and applications [3]–[5], [28]–[30], [44], [47]. From the previous work, we can conclude that conventional FCM is sensitive to noise, although it can take effects on most noise-free images. In order to increase its robustness, many improved FCM-related algorithms have been proposed [1], [2], [9], [11], [12], [20], [22], [24], [26], [27], [32], [38], [40], [47].

For instance, Ahmed *et al.* [2] proposed a novel algorithm called FCM\_S that incorporates spatial constraints to modify the objective function of the conventional FCM algorithm. Although FCM\_S improves the segmentation ability, it is very time consuming for each iteration. To improve its computational efficiency, Chen and Zhang [12] introduced an improved one that formulates two low-complexity variants of FCM\_S by computing the mean or median filtered images in advance. Szilagyi *et al.* [40] reported an enhanced FCM algorithm (EnFCM). The original image pixels and their neighborhood averages are first employed to generate a nonlinearily weighted sum image. Then, the summed image is segmented by using FCM. Thus, EnFCM is not very time consuming. On the basis of EnFCM, Cai *et al.* [11] proposed a fast generalized FCM algorithm. Compared with EnFCM, it innovatively measures the similarity between the original image pixels and their spatial information so as to generate a nonlinearily

weighted sum image. Moreover, its computational efficiency is high.

To further enhance the effectiveness of FCM, kernel-based FCM algorithms have received much attention, aiming to make FCM robust to noise by incorporating the kernel distance measure to the objective function [9], [23]–[25], [38], [47]. Based on this advantage, Gong *et al.* [24] proposed a kernel metric-based FCM algorithm, which depends on local information to assess the damping extent of neighborhood of pixels. It gains successful applications to segment artificial and real images. Elazab *et al.* [20] presented an FCM framework that exploits the heterogeneity of grayscales in the neighborhood for local contextual information and incorporates the Gaussian radial basis kernel function into the objective function.

Recently, Adhikari *et al.* [1] improved the FCM algorithm by incorporating conditional variables and local information into membership functions. It is successfully applied to segment magnetic resonance imaging (MRI) brain images. More recently, Gharieb *et al.* [22] introduced an improved FCM algorithm based on local membership and locally smoothed data incorporating Kullback–Leibler divergence for image segmentation. Compared with the previous approaches, its main motivation is to incorporate spatial information into the hard  $C$ -means algorithm by spatially smoothing membership functions of pixels in the pixel vicinity.

Through the literature review, it can be concluded that the existing algorithms mostly take the spatial information in an image and nonrobust Euclidean distance into account and are solely based on the distribution of image data. Their drawback is that they fail to take the feature space distribution of image data into consideration during the formulation of clusters. Both image features and noise belong to high-frequency information of image data. It is not difficult to consider high and low frequencies as features of image data. There are many ways to acquire such frequency information of image pixels, such as Fourier transform, orthonormal wavelets [14], translation-invariant wavelets [13], and framelets [15], [36]. Unlike the above ways, tight wavelet frames can provide redundant representations of images [18]. This redundancy enables tight wavelet frames to be flexibly applied to various areas, such as image denoising, image restoration, and surface reconstruction [10], [16]–[18], [43], [45]. Motivated by the above analysis, this paper employs tight wavelet frames to form feature spaces of image data defined on graphs. FCM is applied to segment these feature spaces for increasing its robustness. The segmented images on graphs are reconstructed by the wavelet frame transform on graphs. Numerical experiments demonstrate that the approach can effectively remove noise and retain feature details in images on graphs, which means that it has a wider range of applications than other image segmentation algorithms.

### III. PRELIMINARIES

In order to enhance the understanding and analysis of graphs and image data defined on graphs, spectral graph theory [16], [39] is reviewed.

A graph  $G = (V, E, \omega)$  consists of a vertex set  $V := \{v_k : k = 0, \dots, K - 1\}$ , an edge set  $E \subseteq V \times V$ , and a weight function  $\omega : E \mapsto \mathbb{R}^+$  that represents the distance between two adjacent vertices. According to [16], the following expression is commonly used:

$$\omega(v_k, v_{k'}) := e^{-\|v_k - v_{k'}\|^2/\rho}, \quad \rho > 0 \quad (1)$$

where  $v_k$  and  $v_{k'}$  denote two arbitrary vertices in  $V$  and  $\|\cdot\|$  denotes their Euclidean distance. Here,  $v_k = (v_k(1), v_k(2), v_k(3))$  represents the  $(x, y, z)$ -coordinates of vertex  $v_k$ , and the distance between  $v_k$  and  $v_{k'}$  is formulated as  $\|v_k - v_{k'}\| = \sqrt{\sum_{i=1}^3 [v_k(i) - v_{k'}(i)]^2}$ .

The adjacency matrix  $\Phi$  for graph  $G$  is a  $K$ -order sparse matrix, of which entry  $\phi_{k,k'}$  is defined as follows:

$$\phi_{k,k'} = \begin{cases} \omega(v_k, v_{k'}) & \text{if an edge in } E \text{ connects } v_k \text{ and } v_{k'} \\ 0 & \text{otherwise.} \end{cases} \quad (2)$$

Let  $\psi[k] := \sum_{k'} \phi_{k,k'}$  be the degree of each vertex  $v_k$ . Here,  $\psi[k]$  denotes the sum of all the weights between  $v_k$  and its neighbors. All the degrees constitute a degree matrix  $\Psi$  that is described as

$$\Psi := \text{diag}\{\psi[1], \psi[2], \dots, \psi[K]\}. \quad (3)$$

Then, the non-normalized graph Laplacian  $\mathcal{L}$  can be formulated as

$$\mathcal{L} := \Psi - \Phi.$$

By carrying out the eigenvalue decomposition for  $\mathcal{L}$ , the set of  $K$  pairs of its eigenvalues and eigenvectors can be obtained, which is formulated as  $\{(\lambda_k, u_k)\}_{k=0}^{K-1}$ . As  $\mathcal{L}$  is a real symmetric matrix, it can be acquired that  $\lambda_{K-1} \geq \lambda_{K-2} \dots \geq \lambda_2 \geq \lambda_1 > \lambda_0 = 0$ . Here, for all of the functions on  $G$ , the eigenvectors form an orthonormal basis as follows:

$$\langle u_k, u_{k'} \rangle = \sum_{z=0}^{K-1} u_k[z] u_{k'}[z] = \delta_{k,k'}.$$

Let us define a real-valued function  $f : V \mapsto \mathbb{R}$ . Then,  $(f(v_1), f(v_2), \dots, f(v_K))$  can be viewed as a  $K$ -dimensional vector in  $\mathbb{R}^K$ , where  $f(v_k)$  defines a coordinate. In practical applications, it is also represented as a specific object such as an image. Moreover, we have its Fourier transform

$$\widehat{f}[k] := \sum_{z=0}^{K-1} f[z] u_k[z], \quad k = 0, 1, \dots, K - 1.$$

#### A. Wavelet Frame Transform on Graphs

Given a graph  $G := (V, E, \omega)$  and an image function  $f : V \mapsto \mathbb{R}$  on  $G$ . For  $k = 0, 1, \dots, K - 1$ ,  $\{\lambda_k\}$  denotes the set of the eigenvalues of graph Laplacian  $\mathcal{L}$ . The discrete tight wavelet frame transform of  $f$  can be formulated. More details can be found in [16].

For  $p = 0, 1, \dots, r$ ,  $\{a_p\}$  denotes a set of masks.  $\widehat{a}_p$  denotes the Fourier series of  $a_p$ . As  $a_p$  is finitely supported,  $\widehat{a}_p$  can be

described by a trigonometric polynomial. Let  $\widehat{a}_p^*$  be the complex conjugate of  $\widehat{a}_p$ . The (undecimated)  $L$ -level tight wavelet frame decomposition  $\mathcal{W}$  is defined as

$$\mathcal{W}f := \{\mathcal{W}_{p,\ell}f : p = 0, 1, \dots, r, \ell = 1, 2, \dots, L\} \quad (4)$$

where, for  $\ell = 1$

$$\widehat{\mathcal{W}_{p,\ell}f}[k] := \widehat{a}_p^*(2^{-N}\lambda_k)\widehat{f}[k]$$

and for  $\ell \in \{2, 3, \dots, L\}$

$$\widehat{\mathcal{W}_{p,\ell}f}[k] := \widehat{a}_p^*(2^{-N+\ell-1}\lambda_k)\widehat{a}_0^*(2^{-N+\ell-2}\lambda_k)\cdots\widehat{a}_0^*(2^{-N}\lambda_k)\widehat{f}[k].$$

Here,  $p$  denotes the band of the transform,  $\ell$  denotes the level of the transform, and  $N$  is a positive integer and denotes the dilation scale, which is selected such that  $2^{N-1}\pi < \lambda_{K-1} \leq 2^N\pi$ .

For  $p = 0, 1, \dots, r$  and  $\ell = 1, 2, \dots, L$ , let  $\chi := \mathcal{W}f := \{\chi_{p,\ell}\}$  with  $\chi_{p,\ell} := \mathcal{W}_{p,\ell}f$ . For  $\ell = L, L-1, \dots, 1$ , the tight wavelet frame reconstruction  $\mathcal{W}^T\chi$  is defined by the following iterative procedure:

$$\widehat{\chi}_{0,\ell-1}[k] = \sum_{p=0}^r \widehat{a}_p(2^{-N+\ell-1}\lambda_k)\widehat{\chi}_{p,\ell}[k]$$

where  $\chi_{0,0} := \mathcal{W}^T\chi$  is the reconstructed data from  $\chi$ . According to [16, Th. 3.1], we can obtain  $\mathcal{W}^T\mathcal{W}f = f$ , which means that  $\mathcal{W}^T\mathcal{W}$  is an identity operation.

## B. FCM Algorithm

We denote images as vectors in  $\mathbb{R}^N$ , where  $N$  equals to the total number of pixels. Thus, we can formulate an image as  $X = \{\mathbf{x}_1, \mathbf{x}_2, \dots, \mathbf{x}_N\} \subset \mathbb{R}^N$ , FCM splits it into  $c$  clusters by solving the minimization problem with the following objective function:

$$\begin{aligned} J(\mathbf{H}, \mathbf{y}) &= \sum_{j=1}^N \sum_{i=1}^c h_{ij}^m \|\mathbf{x}_j - \mathbf{y}_i\|^2 \\ \text{s.t. } \forall j \in \{1, 2, \dots, N\} : &\sum_{i=1}^c h_{ij} = 1 \\ \forall j \in \{1, 2, \dots, N\}, \forall i \in \{1, 2, \dots, c\} : &h_{ij} \in [0, 1] \end{aligned}$$

where  $\mathbf{H} = [h_{ij}]_{c \times N}$  is a partition matrix,  $m$  is a fuzziness coefficient ( $m > 1$ ),  $c$  is the number of clusters, and  $\|\cdot\|$  denotes the Euclidean distance. The iterative updates of the partition matrix and prototypes are realized as follows [7]:

$$h_{ij} = \frac{\left(\|\mathbf{x}_j - \mathbf{y}_i\|^2\right)^{-\frac{1}{m-1}}}{\sum_{q=1}^c \left(\|\mathbf{x}_j - \mathbf{y}_q\|^2\right)^{-\frac{1}{m-1}}}$$

and

$$\mathbf{y}_i = \frac{\sum_{j=1}^N h_{ij}^m \mathbf{x}_j}{\sum_{j=1}^N h_{ij}^m}.$$

Once the termination  $\|\mathbf{y}^{(t)} - \mathbf{y}^{(t-1)}\| < \varepsilon$  has been met, FCM stops. Here,  $\varepsilon$  denotes a positive threshold,  $t$  is an iteration count of the algorithm.

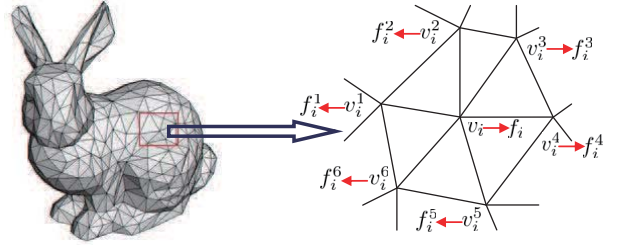


Fig. 2. Graph and its structure.

## IV. METHODOLOGY

### A. Filtering Images on Graphs

Consider a graph  $G := (V, E, \omega)$  and an image function  $f : V \mapsto \mathbb{R}$  on  $G$ . For an image, there exists very high correlation among image pixels. Thus, spatial information should be taken into account for image segmentation. In other words, since an arbitrary image datum  $f_i$  on vertex  $v_i$  and its neighbors  $\{f_i^1, f_i^2, \dots, f_i^6\}$  have similar membership, center  $f_i$  can be filtered by image data on neighboring vertices, which can enhance the robustness of FCM.  $f_i$  and its neighbors  $\{f_i^1, f_i^2, \dots, f_i^6\}$  are shown in Fig. 2.

Formally speaking, a filtered image  $\bar{f}$  can be formulated as

$$\bar{f} = \Psi^{-1}(\Phi f) \quad (5)$$

where  $\Phi$  and  $\Psi$  are defined in (2) and (3), respectively.

### B. Constructing Feature Spaces of Images on Graphs

In the previous section, we have mostly discussed how to filter image data on graphs by using spatial information. In this section, we introduce the process of utilizing tight wavelet frames to construct feature spaces of image data on graph.

Before introducing the construction process, we report on an effective way to enhance the computational efficiency of wavelet frame transform on graphs. As mentioned above, wavelet frame transform involves the eigenvalue decomposition of the graph Laplacian of a graph. In practical applications, it is very challenging to compute all eigenvalues of the graph Laplacian of a large graph. To overcome this problem, Chebyshev polynomials [33] can be employed to approximate the masks of a tight wavelet frame system. In this case, we do not have to calculate all eigenvalues of the graph Laplacian. Moreover, for  $p = 0, 1, \dots, r$ , mask  $a_p$  is a finitely supported sequence. Thus, a low-degree Chebyshev polynomial can be used to accurately approximate  $\widehat{a}_p$  described by a trigonometric polynomial. For  $\xi \in [0, \pi]$ , the approximation of mask  $\widehat{a}_p(\xi)$  is formulated as

$$\widehat{a}_p(\xi) \approx \mathcal{T}_p^n(\xi) = \frac{1}{2}c_{p,0} + \sum_{\zeta=1}^{n-1} c_{p,\zeta} T_\zeta(\xi)$$

where

$$c_{p,\zeta} = \frac{2}{\pi} \int_0^\pi \cos(\zeta\theta) \widehat{a}_p\left(\frac{\pi}{2}(\cos(\theta) + 1)\right) d\theta$$

and

$$T_\zeta(\xi) = \begin{cases} 1 & \zeta = 0 \\ \frac{\xi - \pi/2}{\pi/2} & \zeta = 1 \\ \frac{4}{\pi}(\xi - \pi/2)T_{\zeta-1}(\xi) - T_{\zeta-2}(\xi) & \zeta = 2, 3, \dots \end{cases}$$

The eigenvalue decomposition of  $\mathcal{L}$  is reformulated as  $\mathcal{L} = U\Lambda U^T$ , where  $\Lambda := \text{diag}\{\lambda_0, \lambda_1, \dots, \lambda_{K-1}\}$  and  $U$  contains a group of eigenvectors. Thus, the wavelet frame transform (4) can be represented in the matrix form expressed in the time domain. For  $\ell = 1$

$$\mathcal{W}_{p,\ell}f := U\hat{\mathbf{a}}_p^*(2^{-N}\Lambda)U^T f$$

and for  $\ell \in \{2, 3, \dots, L\}$

$$\mathcal{W}_{p,\ell}f := U\hat{\mathbf{a}}_p^*(2^{-N+\ell-1}\Lambda)\hat{\mathbf{a}}_0^*(2^{-N+\ell-2}\Lambda)\dots\hat{\mathbf{a}}_0^*(2^{-N}\Lambda)U^T f$$

where  $\hat{\mathbf{a}}_p^*(\vartheta\Lambda) := \text{diag}\{\hat{a}_p^*(\vartheta\lambda_0), \hat{a}_p^*(\vartheta\lambda_1), \dots, \hat{a}_p^*(\vartheta\lambda_{K-1})\}$ . If  $\hat{\mathbf{a}}_p$  is substituted with polynomial  $\mathcal{T}_p^n$ , then for  $\ell = 1$

$$\begin{aligned} U\hat{\mathbf{a}}_p^*(2^{-N}\Lambda)U^T f &\approx UT_p^{n*}(2^{-N}\Lambda)U^T f \\ &= \mathcal{T}_p^{n*}(2^{-N}U\Lambda U^T)f = \mathcal{T}_p^{n*}(2^{-N}\mathcal{L})f \end{aligned} \quad (6)$$

and for  $\ell \in \{2, 3, \dots, L\}$

$$\begin{aligned} U\hat{\mathbf{a}}_p^*(2^{-N+\ell-1}\Lambda)\hat{\mathbf{a}}_0^*(2^{-N+\ell-2}\Lambda)\dots\hat{\mathbf{a}}_0^*(2^{-N}\Lambda)U^T f &\approx \mathcal{T}_p^{n*}(2^{-N+\ell-1}\mathcal{L})\mathcal{T}_0^{n*}(2^{-N+\ell-2}\mathcal{L})\dots\mathcal{T}_0^{n*}(2^{-N}\mathcal{L})f. \end{aligned} \quad (7)$$

To compute (6) and (7), only matrix–vector multiplications are involved, which are derived from the iterative definition of the Chebyshev polynomial. Thus, the computation cost is very low. Moreover, the wavelet frame reconstruction  $\mathcal{W}^T \chi$  can also be approximated in a similar way.

According to [36] and [46], the piecewise linear B-spline tight frame system can provide a simple explicit expression to give redundant representations of images, which offers more adaptability to noise. Thus, we choose this system. Formally speaking, the system is formulated as

$$\hat{a}_0(\xi) = \cos^2(\xi/2), \hat{a}_1(\xi) = \frac{1}{\sqrt{2}}\sin(\xi), \hat{a}_2(\xi) = \sin^2(\xi/2).$$

Once tight frame system is determined, we can utilize tight wavelet frames to form feature spaces of image data on graphs, that is,  $X = \mathcal{W}f$  and  $\bar{X} = \mathcal{W}\bar{f}$ , where  $X = \{x_1, x_2, \dots, x_N\}$  is the set of feature vectors associated with the image function  $f$ ,  $\bar{X} = \{\bar{x}_1, \bar{x}_2, \dots, \bar{x}_N\}$  is that with filtered image function  $\bar{f}$  obtained via (5) and  $\mathcal{W}$  is the  $L$ -level tight wavelet frame decomposition whose detailed computation is shown in (6) and (7).

In order to visually judge the feature (edge) extraction ability of tight wavelet frames, we here show a numerical example, refer to Fig. 3. As most images have some geometrical structures, the edges of images are not randomly distributed. Fig. 3 illustrates the map of image edges detected by tight wavelet frames. Clearly, by using tight wavelet frames, image edges are spatially described and correlated. Motivated by the performance of tight wavelet frames, this paper aims at investigating a wavelet frame-based FCM algorithm which can segment images defined in nonflat domains.

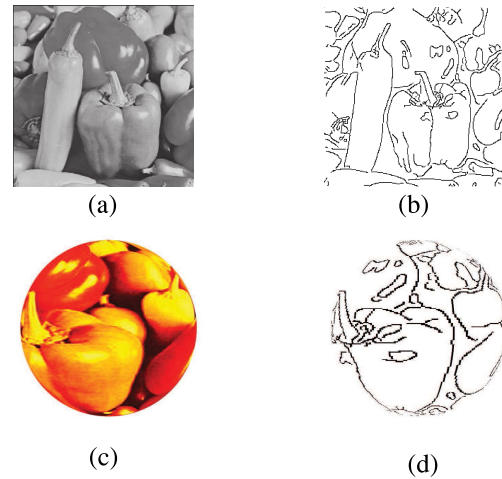


Fig. 3. Illustration of the map of image edges detected by tight wavelet frames. (a) Original grayscale image. (b) Original binary image. (c) Image  $f$  on a sphere. (d) Binary image of  $\mathcal{W}f$ .

Notice that both  $X$  and  $\bar{X}$  describe feature spaces between the observed image data and the filtered image data on graphs, that is, high and low frequency information, which means that underlying image features (edges) and noise can be found. However, the dimensionality of image data increases while forming feature spaces. Due to complexity of data space, the implementation of FCM becomes challenging.

### C. Tight Wavelet Frames-Based FCM Algorithm

In this section, combining feature spaces between the observed image data and the filtered image data on graphs, that is,  $X = \mathcal{W}f$  and  $\bar{X} = \mathcal{W}\bar{f}$ , where  $X = \{x_1, x_2, \dots, x_N\}$  and  $\bar{X} = \{\bar{x}_1, \bar{x}_2, \dots, \bar{x}_N\}$ , we propose a wavelet frame-based FCM algorithm by solving the minimization problem with the following objective function:

$$\begin{aligned} J(\mathbf{H}, \mathbf{y}) &= \sum_{j=1}^N \sum_{i=1}^c h_{ij}^m (\|x_j - y_i\|^2 + \mu \|\bar{x}_j - y_i\|^2)^{-\frac{1}{m-1}} \\ \text{s.t. } \forall j \in \{1, 2, \dots, N\} : \sum_{i=1}^c h_{ij} &= 1 \\ \forall j \in \{1, 2, \dots, N\}, \forall i \in \{1, 2, \dots, c\} : h_{ij} &\in [0, 1] \end{aligned} \quad (8)$$

where objective function  $J(\mathbf{H}, \mathbf{y})$  in (8) for image segmentation in a Euclidean space was first introduced in [12]. Parameter  $\mu$  is used to control the effect of the neighboring term.

Taking into account (8), we have the following iterative solutions:

$$h_{ij} = \frac{\left( \|x_j - y_i\|^2 + \mu \|\bar{x}_j - y_i\|^2 \right)^{-\frac{1}{m-1}}}{\sum_{q=1}^c \left( \|x_j - y_q\|^2 + \mu \|\bar{x}_j - y_q\|^2 \right)^{-\frac{1}{m-1}}} \quad (9)$$

and

$$y_i = \frac{\sum_{j=1}^N h_{ij}^m (x_j + \mu \bar{x}_j)}{(1 + \mu) \sum_{j=1}^N h_{ij}^m}. \quad (10)$$

With  $t$  iterations, once  $\|\mathbf{y}^{(t)} - \mathbf{y}^{(t-1)}\| < \varepsilon$  is met, the proposed algorithm stops. The segmentation computation process is realized in Algorithm 1.

**Algorithm 1** Tight Wavelet Frames-Based FCM Algorithm

**Input:** Image  $f$ , fuzziness coefficient  $m$ , number of clusters  $c$ , and threshold  $\varepsilon$ .  
**Output:** Segmented image  $\tilde{f}$ , prototypes  $y_i$ , and partition matrix  $H$ .

- 1: Calculate filtered image  $\bar{f}$  via (5)
- 2: Calculate  $\mathcal{W}f$  and  $\mathcal{W}\bar{f}$  to obtain feature sets  $X$  and  $\bar{X}$  via (6) and (7)
- 3: Initialize randomly prototypes  $y_i^{(0)}$ .
- 4:  $t \leftarrow 1$
- 5: **repeat**
- 6:   Calculate partition matrix  $H^{(t)}$  using prototypes  $y_i^{(t-1)}$  via (9)
- 7:   Update the prototypes to obtain  $y_i^{(t)}$  by using partition matrix  $H^{(t)}$  via (10)
- 8:    $t \leftarrow t + 1$
- 9: **until**  $\|y_i^{(t)} - y_i^{(t-1)}\| < \varepsilon$
- 10: **return** prototypes  $y_i$  and partition matrix  $H$
- 11: Calculate segmented image  $\tilde{f}$  by using wavelet frame reconstruction  $\mathcal{W}^T$

To quantitatively show the segmentation ability of the proposed algorithm, we adopt the segmentation accuracy as an assessment criterion, that is

$$SA = \sum_{i=1}^c \frac{|B_i \cap C_i|}{\sum_{j=1}^c |C_j|} \quad (11)$$

where  $C_i$  denotes the set of the  $i$ th cluster in the ground-truth segmented image data on graphs,  $B_i$  indicates the set of image data belonging to the  $i$ th cluster found by the test algorithm, and  $|\cdot|$  stands for the cardinality of the set.

## V. EXPERIMENTAL STUDY

In the previous section, we have discussed the methodology for segmenting images on graphs. In this section, some supporting numerical experiments are provided to test the segmentation quality of the proposed algorithm. In Section II, we mention many improved FCM-related algorithms. Especially, Gong *et al.* [24] presented a kernel metric-based FCM algorithm to enhance FCM's robustness. Adhikari *et al.* [1] proposed a conditional FCM algorithm and successfully apply it to segment MRI brain images. More recently, Gharieb *et al.* [22] proposed an improved FCM algorithm based on local membership and locally smoothed data incorporating Kullback–Leibler divergence for image segmentation. For the sake of concise exposition, these algorithms mentioned above and the proposed algorithm are abbreviated as “ $\alpha$ -FCM,” “ $\beta$ -FCM,” “ $\gamma$ -FCM,” and “W-FCM,” respectively. We make comparisons between W-FCM and other algorithms,  $\alpha$ -FCM,  $\beta$ -FCM, and  $\gamma$ -FCM. The comparisons are done both visually and quantitatively. All experiments are implemented in MATLAB on a laptop with Intel Core i3 (2.10 GHz) CPU and 6.0-GB RAM.

For parameter setting, we experimentally set  $n = 8$  in (6), which means that mask  $\hat{a}_p$  is approximated by the Chebyshev polynomials of degree 7. In addition, we choose parameter

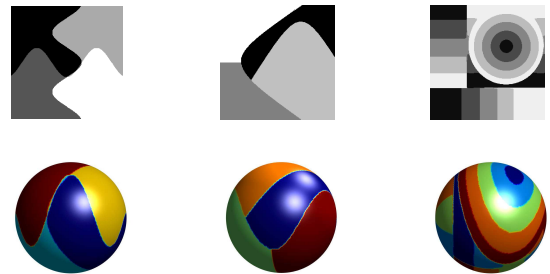


Fig. 4. Three images (first row), mapped onto a unit sphere (second row). From left to right: first image, second image, and third image.

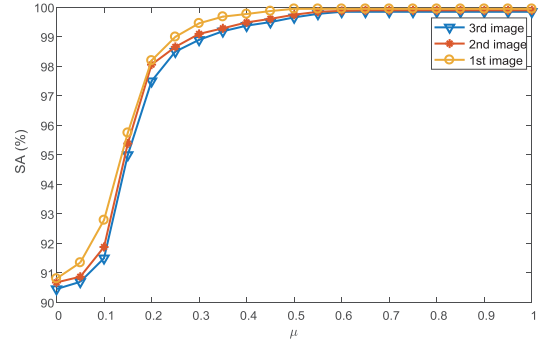


Fig. 5. Segmentation accuracy values with changes of  $\mu$ .

$\rho = 10$  in (1). In (8), we choose the degree of fuzziness  $m = 2$ . In Algorithm 1, we set the threshold  $\varepsilon = 1 \times 10^{-6}$ .

### A. Results for Synthetic Images on Graphs

The above algorithms are employed to test synthetic images on graphs. As shown in Fig. 4, we first map three images onto a unit sphere to generate image data defined on graphs. The numbers of clusters are 4, 4, and 5, respectively. Here, we select the unit sphere with 40 962 sampled vertices as the graph from which one can visually judge denoising quality easily. Noisy-free images are rescaled to an intensity ranging from 0 to 255. We use the MATLAB function “imnoise” to add additive white Gaussian noise (AWGN) and salt and pepper impulse noise (SPIN) of different intensities. The PN is added by using the MATLAB function “poissrnd.” Moreover, we also generate mixed Poisson–Gaussian noise (MPGN) and mixed Gaussian and impulse noise (MGIN). We perform the segmentation with the proposed and other algorithms obtain the results as shown in Figs. 7–9. In addition, we quantitatively show their segmentation performances in Tables I and II in terms of the segmentation accuracy defined by (11). According to [12],  $\mu$  is determined experimentally with  $\mu \in [0.55, 0.65]$ . For selection of  $\mu$  in (8), we take a set of its values to test its effect on the performance with the three images on the unit sphere contaminated by 20% SPIN. As shown in Fig. 5, for the three images, there are no apparent changes by setting  $\mu = 0.65$ , which implies that the performance is rather stable. Here, as an example, we consider the third image on the unit sphere contaminated by AWGN of different intensities (standard deviations) to test segmentation accuracy *vis-à-vis* changes of tight wavelet frame transform level  $\ell$ . As shown

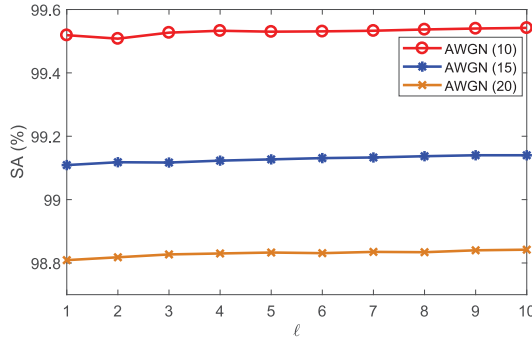


Fig. 6. Segmentation accuracy values with changes of  $\ell$ .

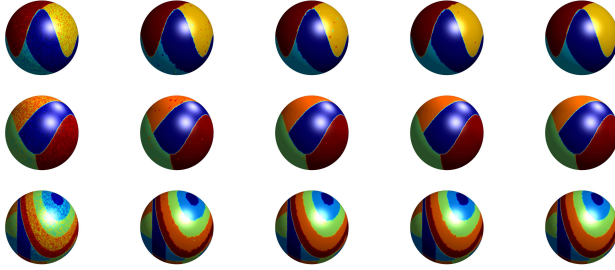


Fig. 7. Segmentation results with AWGN (standard deviation = 20,  $\mu_1 = 0.55$ ,  $\mu_2 = 0.60$ , and  $\mu_3 = 0.65$ ). From left to right: noisy images on graphs, and results with  $\alpha$ -FCM,  $\beta$ -FCM,  $\gamma$ -FCM, and W-FCM.

in Fig. 6, it is concluded that we just need to use 1-level wavelet frame transformation in all experiments, since the use of higher decomposition levels only slightly enhances the segmentation performance while the computational efficiency is significantly reduced.

Fig. 7 shows the segmentation results of these four algorithms in the presence of AWGN (standard deviation = 20). On the one hand, it is not difficult to find that the denoising results of  $\alpha$ -FCM and  $\beta$ -FCM are unsatisfactory. Particularly,  $\alpha$ -FCM has bad performance while denoising AWGN. Visually, as  $\gamma$ -FCM removes a large proportion of noise, it is superior to  $\alpha$ -FCM and  $\beta$ -FCM. However,  $\gamma$ -FCM cannot remove noise and preserve image features completely. On the other hand, W-FCM not only has good performance in the presence of AWGN but also retain much more image features than the others.

Fig. 8 illustrates the segmentation results of these four algorithms in the presence of SPIN (density = 20%). The results of  $\alpha$ -FCM show that it cannot completely remove noise in images, but keep clear edges. Similarly, the denoising results of  $\beta$ -FCM are unsatisfactory. Visually, compared with  $\alpha$ -FCM and  $\beta$ -FCM,  $\gamma$ -FCM has better performance to remove noise, since it can accurately estimate the relationship among neighbors. Unfortunately, it changes image edges. We can conclude that the above three algorithms cannot simultaneously remove noise and retain image feature details. W-FCM overcomes this drawback and performs better than the others.

Fig. 9 presents the segmentation results of these four algorithms in the presence of PN. Visually, although  $\alpha$ -FCM removes a large proportion of noise, the results are unsatisfactory. Compared with  $\alpha$ -FCM, both  $\beta$ -FCM and  $\gamma$ -FCM have

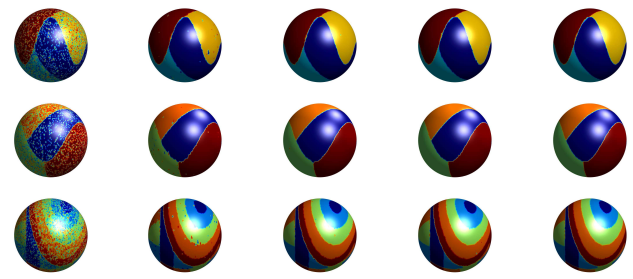


Fig. 8. Segmentation results with SPIN (density = 20%,  $\mu_1 = 0.55$ ,  $\mu_2 = 0.60$ , and  $\mu_3 = 0.65$ ). From left to right: noisy images on graphs, and results with  $\alpha$ -FCM,  $\beta$ -FCM,  $\gamma$ -FCM, and W-FCM.

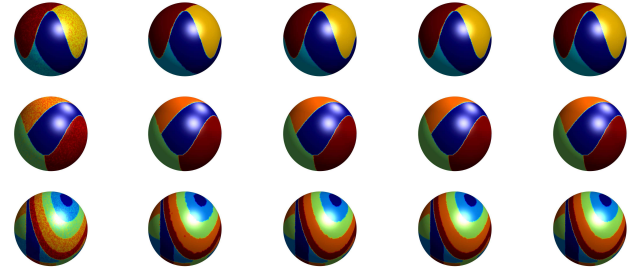


Fig. 9. Segmentation results with PN ( $\mu_1 = 0.55$ ,  $\mu_2 = 0.60$ , and  $\mu_3 = 0.65$ ). From left to right: noisy images on graphs, and results with  $\alpha$ -FCM,  $\beta$ -FCM,  $\gamma$ -FCM, and W-FCM.

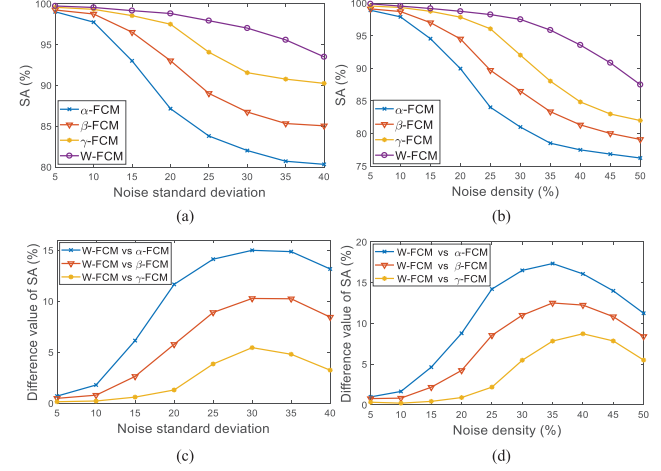


Fig. 10. Segmentation accuracy results of the third image on a synthetic graph ( $\mu = 0.65$ ). (a) Standard deviations of AWGN. (b) Densities of SPIN. (c) Proposed and other algorithms versus AWGN standard deviations. (d) Proposed and other algorithms versus SPIN densities.

better performance to remove noise. However, W-FCM retains more image feature details than the other three algorithms.

Fig. 10(a) and (b) gives the changing curves of segmentation accuracy values of these four algorithms in the presence of AWGN and SPIN of different intensities, respectively. The range of AWGN levels is from 5 to 40. The range of SPIN levels is from 5% to 50%. In multiple experiments, we set  $\mu$  to 0.65. It is obviously seen that the segmentation accuracy values of W-FCM are greater than those of other algorithms in the presence of different noise intensities. Fig. 10(c) and (d) provides their changing curves of the corresponding difference

TABLE I  
SEGMENTATION ACCURACY VALUES (%) ON DIFFERENT IMAGES  
WITH DIFFERENT LEVELS OF NOISE

Image	Noise level	$\alpha$ -FCM	$\beta$ -FCM	$\gamma$ -FCM	W-FCM
1	AWGN(10)	97.852	98.432	99.378	99.737
	AWGN(20)	87.954	93.453	97.257	99.636
	AWGN(30)	82.356	86.785	92.366	97.869
	SPIN(10%)	98.547	98.815	99.536	99.800
	SPIN(20%)	90.906	94.958	97.539	98.885
	SPIN(30%)	81.127	87.244	92.853	98.224
	PN	96.874	98.517	98.082	99.424
2	AWGN(10)	97.324	98.563	99.245	99.634
	AWGN(20)	87.978	93.335	97.826	99.245
	AWGN(30)	82.726	87.536	92.945	98.378
	SPIN(10%)	97.632	98.278	99.392	99.699
	SPIN(20%)	90.205	94.635	97.421	98.869
	SPIN(30%)	82.034	87.154	92.645	97.853
	PN	97.128	98.634	99.085	99.522
3	AWGN(10)	97.762	98.753	99.326	99.553
	AWGN(20)	87.485	93.032	97.755	98.857
	AWGN(30)	82.280	86.747	91.563	97.059
	SPIN(10%)	97.655	98.532	99.266	99.578
	SPIN(20%)	90.105	94.646	97.680	98.862
	SPIN(30%)	82.015	86.855	92.538	97.536
	PN	94.376	97.424	98.976	99.424

TABLE II  
SEGMENTATION ACCURACY VALUES (%) ON  
DIFFERENT IMAGES WITH MIXED NOISES

Image	Noise level	$\alpha$ -FCM	$\beta$ -FCM	$\gamma$ -FCM	W-FCM
1	MPGN(10)	93.352	96.757	97.531	99.012
	MPGN(20)	86.831	92.754	96.779	97.337
	MPGN(30)	81.585	85.380	90.934	96.162
	MGIN(10, 10%)	96.550	97.568	98.130	99.194
	MGIN(10, 20%)	89.917	93.076	96.569	97.311
	MGIN(10, 30%)	81.286	85.054	91.469	96.529
	MPGN(10)	93.166	96.451	97.538	99.005
2	MPGN(20)	86.602	92.084	96.996	97.775
	MPGN(30)	81.263	85.229	90.078	96.817
	MGIN(10, 10%)	96.654	97.913	98.443	99.069
	MGIN(10, 20%)	89.689	93.152	96.107	97.084
	MGIN(10, 30%)	81.748	85.826	91.962	96.400
	MPGN(10)	93.260	96.146	97.853	99.240
	MPGN(20)	86.800	92.136	96.622	97.123
3	MPGN(30)	81.431	85.869	90.351	96.184
	MGIN(10, 10%)	96.911	97.580	98.513	99.040
	MGIN(10, 20%)	89.182	93.550	96.402	97.417
	MGIN(10, 30%)	81.264	85.145	91.076	96.050

values of segmentation accuracy. The difference values come up to the maxima when the image is corrupted by 30 AWGN or 35% SPIN. Experimental results show that W-FCM has higher adaptability to noise and a better performance for segmentation of images on graphs than other FCM-related algorithms.

Table I shows segmentation accuracy values of four algorithms mentioned above in the presence of AWGN, SPIN, and PN. AWGN levels are 10, 20, and 30. SPIN levels are 10%, 20%, and 30%. It is obviously seen that SA values of W-FCM are greater than those of other algorithms in the presence of noise with varying intensities. Notice that the segmentation accuracy value of W-FCM comes up to 99.800% for the case with 10% SPIN on the first image.

Table II includes segmentation accuracy achieved in the presence of mixed noises of different intensities. The two most commonly used types of mixed noises are MPGN and MGIN. The MPGN levels are 10, 20, and 30. The MGIN levels are 10%, 20%, and 30% with fixed ten AWGN. Clearly, the segmentation accuracy of W-FCM is greater than those produced by the others alternatives. Notice that the segmentation

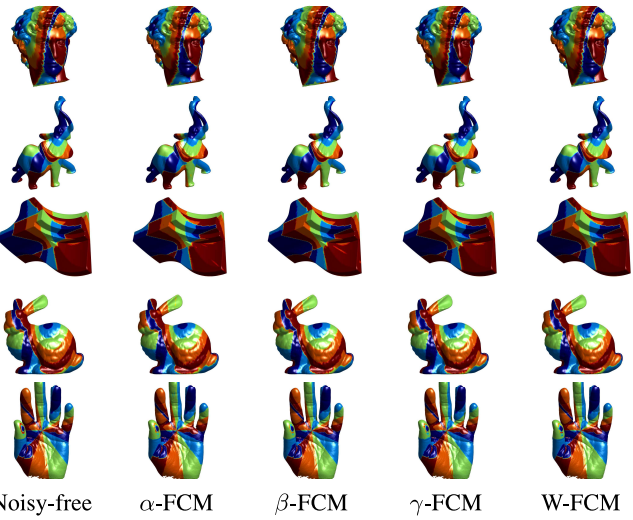


Fig. 11. Segmentation results with AWGN (standard deviation = 20). From left to right: noisy-free images on graphs, and results with  $\alpha$ -FCM,  $\beta$ -FCM,  $\gamma$ -FCM, and W-FCM.

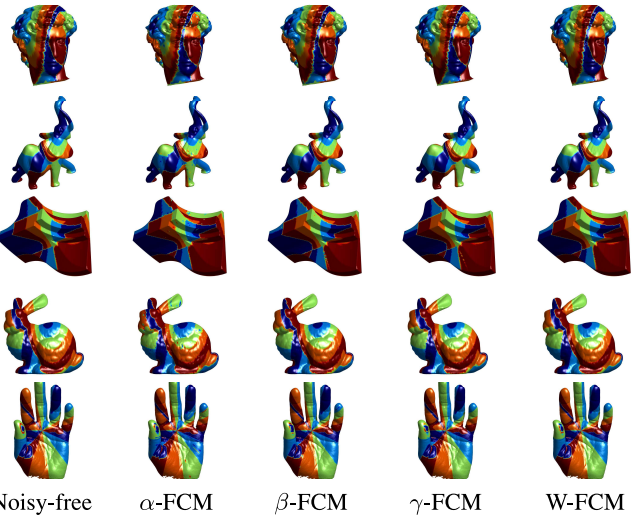


Fig. 12. Segmentation results with SPIN (density = 20%). From left to right: noisy-free images on graphs, and results with  $\alpha$ -FCM,  $\beta$ -FCM,  $\gamma$ -FCM, and W-FCM.

accuracy value of W-FCM comes up to 99.240% for the case with ten MPGN on the third image.

For demonstration of multiphase image segmentation, we also consider five publicly available graphs. These graphs are obtained from “<http://3dmdb.com/>.” We map the third image onto the graphs to generate image data on graphs. The numbers of clusters are all 5. As cluster  $c$  decreases, the percentage of misclassified image data is going to raise. When we set  $c > 5$ , the percentage of misclassified image data tends to be stable. Similarly, we also test the performance of the same four algorithms for segmenting images on graphs corrupted by AWGN, SPIN, PN, and mixed noises, both visually and quantitatively.

Fig. 11 illustrates the segmentation results in the presence of AWGN (standard deviation = 20). The results show that W-FCM can remove much more noise and preserve

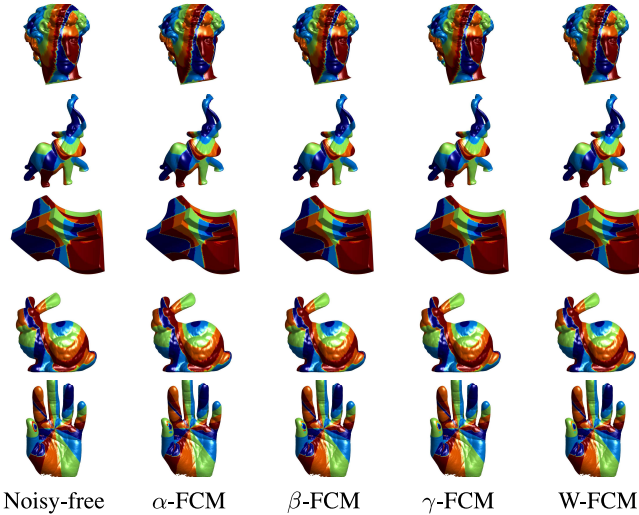


Fig. 13. Segmentation results with PN. From left to right: noisy-free images on graphs, and results with  $\alpha$ -FCM,  $\beta$ -FCM,  $\gamma$ -FCM, and W-FCM.

TABLE III  
SEGMENTATION ACCURACY VALUES (%) ON DIFFERENT  
GRAPHS WITH DIFFERENT LEVELS OF NOISE

Graph	Noise level	$\alpha$ -FCM	$\beta$ -FCM	$\gamma$ -FCM	W-FCM
david-head	AWGN(10)	97.655	97.823	98.766	99.355
	AWGN(20)	87.171	93.695	97.795	98.276
	AWGN(30)	82.706	86.317	91.187	97.680
	SPIN(10%)	97.032	98.550	99.090	99.555
	SPIN(20%)	90.277	95.034	97.446	98.163
	SPIN(30%)	82.046	86.439	92.646	97.119
	PN	94.097	97.382	98.709	99.498
elephant	AWGN(10)	96.960	97.699	98.841	99.251
	AWGN(20)	87.340	93.891	97.254	98.616
	AWGN(30)	82.585	86.959	91.814	97.473
	SPIN(10%)	97.224	98.547	99.244	99.352
	SPIN(20%)	90.751	94.139	97.929	98.831
	SPIN(30%)	82.255	86.149	92.350	97.585
	PN	94.506	97.258	98.197	99.550
fandisk	AWGN(10)	96.917	97.354	98.812	99.402
	AWGN(20)	87.286	93.531	97.337	98.263
	AWGN(30)	82.757	86.779	91.162	97.654
	SPIN(10%)	97.754	98.934	99.194	99.389
	SPIN(20%)	90.380	94.130	97.311	98.748
	SPIN(30%)	82.568	86.569	92.529	97.451
	PN	94.076	97.469	98.166	99.084
bunny	AWGN(10)	97.229	98.443	99.084	99.264
	AWGN(20)	87.913	93.107	97.400	98.146
	AWGN(30)	82.152	86.962	91.260	97.136
	SPIN(10%)	97.826	98.005	99.103	99.669
	SPIN(20%)	90.538	94.775	97.431	98.580
	SPIN(30%)	82.996	86.817	92.911	97.550
	PN	94.078	97.869	98.182	99.145
hand-olivier	AWGN(10)	96.853	97.123	98.491	99.390
	AWGN(20)	87.622	94.184	97.489	98.242
	AWGN(30)	82.351	86.240	91.338	97.404
	SPIN(10%)	97.513	98.417	99.096	99.566
	SPIN(20%)	90.402	94.050	97.369	98.132
	SPIN(30%)	82.076	86.903	92.111	97.942
	PN	94.240	97.945	98.780	99.456

much clearer edges than other algorithms. Similarly, Fig. 12 shows the segmentation results of these four algorithms in the presence of SPIN (density = 20%). Fig. 13 presents the segmentation results of these four algorithms in the presence of PN. W-FCM has a better segmentation ability than the others. Tables III and IV quantitatively show segmentation accuracy values of four algorithms mentioned above in the presence of AWGN, SPIN, PN, and mixed noises. Clearly, segmentation

TABLE IV  
SEGMENTATION ACCURACY VALUES (%) ON DIFFERENT  
GRAPHS WITH MIXED NOISES

Graph	Noise level	$\alpha$ -FCM	$\beta$ -FCM	$\gamma$ -FCM	W-FCM
david-head	MPGN(10)	93.575	96.043	97.547	99.068
	MPGN(20)	86.060	92.169	96.296	97.626
	MPGN(30)	81.235	85.649	90.745	96.780
	MGIN(10, 10%)	96.353	97.732	98.189	99.081
	MGIN(10, 20%)	89.821	93.648	96.687	97.929
	MGIN(10, 30%)	81.015	85.451	91.184	96.776
	MPGN(10)	93.487	96.818	97.351	98.908
elephant	MPGN(20)	86.436	92.795	96.939	97.301
	MPGN(30)	81.447	85.644	90.876	96.471
	MGIN(10, 10%)	96.306	97.379	98.550	99.230
	MGIN(10, 20%)	89.509	93.812	96.622	97.844
	MGIN(10, 30%)	81.511	85.533	91.587	96.195
	MPGN(10)	93.226	96.430	97.258	99.222
	MPGN(20)	86.171	92.185	96.409	97.517
fandisk	MPGN(30)	81.228	85.905	90.595	96.297
	MGIN(10, 10%)	96.436	97.980	98.262	99.119
	MGIN(10, 20%)	89.311	93.439	96.603	97.424
	MGIN(10, 30%)	81.923	85.111	91.711	96.508
	MPGN(10)	93.786	96.489	97.521	98.967
	MPGN(20)	86.262	92.579	96.232	97.958
	MPGN(30)	81.801	85.237	90.489	96.038
bunny	MGIN(10, 10%)	96.029	97.459	98.624	99.085
	MGIN(10, 20%)	89.929	93.963	96.679	97.913
	MGIN(10, 30%)	81.730	85.547	91.396	96.796
	MPGN(10)	93.099	96.707	97.891	99.022
	MPGN(20)	86.262	92.654	96.334	97.480
	MPGN(30)	81.335	85.494	90.699	96.905
	MGIN(10, 10%)	96.680	97.779	98.198	98.910
hand-olivier	MGIN(10, 20%)	89.137	93.715	97.031	97.618
	MGIN(10, 30%)	81.721	85.904	91.744	96.859

accuracy values of W-FCM are greater than those of the others. Notice that the segmentation accuracy value of W-FCM comes up to 99.669% with 10% SPIN on graph “bunny”.

### B. Results for Real Images on Graphs

In the following experiments, we consider publicly available images on graphs, that is, Global Earth observation data. Such data can be interpreted as images given on a sphere, which are borrowed from the NASA Earth Observation dataset: <http://neo.sci.gsfc.nasa.gov/>. Sampled images data contain unknown noise. For the segmentation, we use the RGB color space. To demonstrate multiphase image segmentation, we segment two groups of images on graphs showing both outgoing longwave radiation and sea ice and snow extent, refer to Figs. 14 and 15.

Fig. 14 shows the results of segmenting images showing outgoing longwave radiation. The colors show the amount of outgoing longwave radiation leaving earth's atmosphere per month (from top to bottom: March, June, September, and December 2018). Bright yellow and orange indicate greater heat emission (around 250–350 W/m<sup>2</sup>), purple and blue indicate intermediate emissions (around 150–250 W/m<sup>2</sup>), and white shows little or no heat emission (around 85–150 W/m<sup>2</sup>, negligible). Thus, we set the number of clusters to 2. The segmentation results of  $\beta$ -FCM and  $\gamma$ -FCM show that the two algorithms cannot completely remove noise in images, but keep clear edges. On the contrary, the segmentation results of  $\alpha$ -FCM indicate that several topology changes (splitting and merging) occur during the segmentation. However, W-FCM can not only remove noise but also retain topological edges.

Fig. 15 illustrates the segmentation results with respect to sea ice and snow extent. The colors on this collection

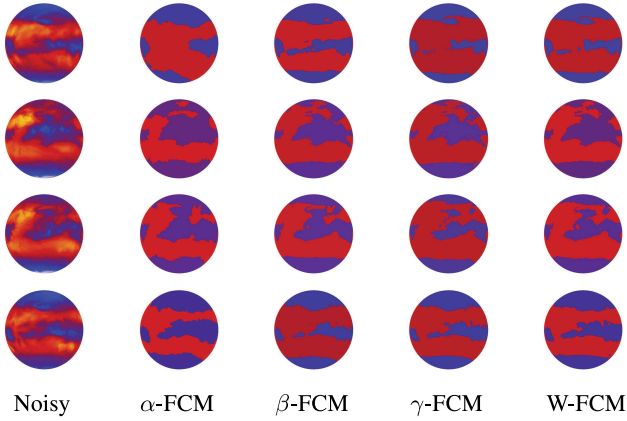


Fig. 14. Segmentation results of outgoing longwave radiation data ( $\mu = 0.60$ ). From left to right: noisy images on graphs, and results with  $\alpha$ -FCM,  $\beta$ -FCM,  $\gamma$ -FCM, and W-FCM. From top to bottom: March, June, September, and December 2018.

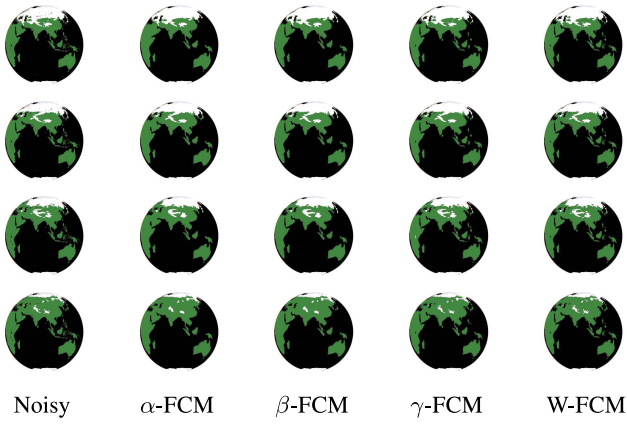


Fig. 15. Segmentation results of sea ice and snow extent data ( $\mu = 0.65$ ). From left to right: noisy images on graphs, and results with  $\alpha$ -FCM,  $\beta$ -FCM,  $\gamma$ -FCM, and W-FCM. From top to bottom: February 7–14, March 7–14, April 4–11, and May 2–9, 2015.

of images show where the land and ocean are covered by snow and ice per week (from top to bottom: February 7–14, March 7–14, April 4–11, and May 2–9, 2015). White shows where earth's lands are covered by snow. Light blue shows where earth's oceans are covered by ice. Green shows lands with no snow cover and black areas show oceans with no ice cover. Thus, we set the number of clusters to 4. For other three FCM-related algorithms, we observe that the noise is well smoothed out. However, these three algorithms change the topological boundaries more or less, informing weak edges. For these practical examples, it is concluded that the above three algorithms cannot simultaneously remove noise and retain image feature details. W-FCM overcomes this drawback and performs better than the other methods.

All the numerical results indicate that W-FCM cannot only remove noise but also retain much more image feature details. Furthermore, it does not depend on the type of noise.

Finally, Table V shows the computational cost on different graphs with four algorithms. We artificially added 20%

TABLE V  
COMPUTATIONAL COST (IN SEC.) ON DIFFERENT GRAPHS

Graph	Data points	$\alpha$ -FCM	$\beta$ -FCM	$\gamma$ -FCM	W-FCM
david-head	23889	126	245	120	253
elephant	24955	130	249	125	261
fandisk	25894	133	253	124	265
bunny	34817	185	354	165	383
hand-olivier	195946	807	1099	613	1425

SPIN to images on graphs. Among them,  $\gamma$ -FCM is the least time consuming. Since the computation of the wavelet frame transform increases the data space, the proposed algorithm is the most time consuming. Nevertheless, on account of its better performance for segmentation of images on graphs than other algorithms, this drawback can be tolerated. In conclusion, compared with other FCM-related algorithms, the W-FCM exhibits a wide range, almost 0.4%–16%, of improvements on segmentation accuracy values in the presence of various levels of noise. Furthermore, as tight wavelet frames provide a new way to analyze and manipulate data effectively, the proposed algorithm can be further applied to other similar fields.

## VI. CONCLUSION

As many practical applications emerge, image processing in irregular domains, such as graphs has received much attention. It provides new insights into signal processing. In this paper, we propose a wavelet frame-based FCM algorithm for segmenting images on graphs. To enhance the robustness of the original FCM algorithm, image data on graphs are filtered by using spatial information. Since a tight wavelet frame system is able to give redundant representations of images, we can utilize it to obtain feature spaces of images on graphs. Combining the original and filtered features, the FCM algorithm is used for segmenting images on graphs contaminated by noise of different intensities. The effectiveness of the algorithm is presented through numerical experiments. Finally, the following conclusions are drawn.

- 1) Tight wavelet frames-based FCM algorithm has acceptable computation complexity. Although it has slightly higher computational cost, its good performance can offset this drawback.
- 2) Tight wavelet frames have high adaptability to image data and noise one and can be used to analyze the characteristics of noise. Therefore, a tight wavelet frames-based FCM algorithm can effectively remove noise and retain feature details in images on graphs.
- 3) Numerical results demonstrate that the proposed tight wavelet frames-based FCM algorithm has better segmentation ability than other FCM-related algorithms. Therefore, the proposed algorithm has a wider range of applications.

Numerical experimental results indicate that the proposed algorithm can be effectively realized in practice. It can be applied to other similar fields. There are some open problems worth pursuing. For example, in a future study, its application areas could be expanded by involving computer networks, social networks, or transportation networks [31], which can all

be visualized as graphs in which the vertices stand for individual computers, people, or cities, respectively. Moreover, more real-world noisy data could be handled with the proposed algorithm so as to describe the effects of removing the measured noise in images on graphs more effectively.

## REFERENCES

- [1] S. K. Adhikari, J. K. Sing, D. K. Basu, and M. Nasipuri, "Conditional spatial fuzzy C-means clustering algorithm for segmentation of MRI images," *Appl. Soft Comput.*, vol. 34, pp. 758–769, Sep. 2015.
- [2] M. N. Ahmed, S. M. Yamany, N. Mohamed, A. A. Farag, and T. Moriarty, "A modified fuzzy C-means algorithm for bias field estimation and segmentation of MRI data," *IEEE Trans. Med. Imag.*, vol. 21, no. 3, pp. 193–199, Mar. 2002.
- [3] X. Bai, Z. Chen, Y. Zhang, Z. Liu, and Y. Lu, "Infrared ship target segmentation based on spatial information improved FCM," *IEEE Trans. Cybern.*, vol. 46, no. 12, pp. 3259–3271, Dec. 2016.
- [4] X. Bai, Y. Zhang, H. Liu, and Z. Chen, "Similarity measure-based possibilistic FCM with label information for brain MRI segmentation," *IEEE Trans. Cybern.*, vol. 49, no. 7, pp. 2618–2630, Jul. 2019.
- [5] S. Balla-Arabé, X. Gao, and B. Wang, "A fast and robust level set method for image segmentation using fuzzy clustering and lattice Boltzmann method," *IEEE Trans. Cybern.*, vol. 44, no. 3, pp. 910–920, Jun. 2013.
- [6] J. C. Bezdek, *Pattern Recognition With Fuzzy Objective Function Algorithms*. New York, NY, USA: Plenum Press, 1981.
- [7] J. C. Bezdek, R. Ehrlich, and W. Full, "FCM: The fuzzy C-means clustering algorithm," *Comput. Geosci.*, vol. 10, nos. 2–3, pp. 191–203, 1984.
- [8] H. Benninghoff and H. Garcke, "Segmentation and restoration of images on surfaces by parametric active contours with topology changes," *J. Math. Imag. Vis.*, vol. 55, no. 1, pp. 105–124, May 2016.
- [9] A. Bouchachia and W. Pedrycz, "Enhancement of fuzzy clustering by mechanisms of partial supervision," *Fuzzy Sets Syst.*, vol. 157, no. 13, pp. 1733–1759, Jul. 2006.
- [10] J. F. Cai, B. Dong, S. Osher, and Z. Shen, "Image restoration: Total variation, wavelet frames, and beyond," *J. Amer. Math. Soc.*, vol. 25, no. 4, pp. 1033–1089, May 2012.
- [11] W. Cai, S. Chen, and D. Zhang, "Fast and robust fuzzy C-means clustering algorithms incorporating local information for image segmentation," *Pattern Recognit.*, vol. 40, no. 3, pp. 825–838, Mar. 2007.
- [12] S. Chen and D. Zhang, "Robust image segmentation using FCM with spatial constraints based on new kernel-induced distance measure," *IEEE Trans. Syst., Man, Cybern. B, Cybern.*, vol. 34, no. 4, pp. 1907–1916, Aug. 2004.
- [13] R. R. Coifman and D. L. Donoho, "Translation-invariant de-noising," in *Wavelets and Statistics* (Lecture Notes in Statistics), A. Antoniadis and G. Oppenheim, Eds. New York, NY, USA: Springer, 1995, pp. 125–150.
- [14] I. Daubechies, *Ten Lectures on Wavelets*, vol. 61. Philadelphia, PA, USA: SIAM, 1992.
- [15] I. Daubechies, B. Han, A. Ron, and Z. Shen, "Framelets: MRA-based constructions of wavelet frames," *Appl. Comput. Harmon. Anal.*, vol. 14, no. 1, pp. 1–46, Jan. 2003.
- [16] B. Dong, "Sparse representation on graphs by tight wavelet frames and applications," *Appl. Comput. Harmon. Anal.*, vol. 42, no. 3, pp. 452–479, May 2017.
- [17] B. Dong, Q. T. Jiang, C. Q. Liu, and Z. Shen, "Multiscale representation of surfaces by tight wavelet frames with applications to denoising," *Appl. Comput. Harmon. Anal.*, vol. 41, no. 2, pp. 561–589, Sep. 2016.
- [18] B. Dong and Z. Shen, "MRA-based wavelet frames and applications," in *The Mathematics of Image Processing* (IAS Lecture Notes Series). Salt Lake City, UT, USA: Park City Math. Inst., 2010.
- [19] J. C. Dunn, "A fuzzy relative of the ISODATA process and its use in detecting compact well-separated clusters," *J. Cybern.*, vol. 3, no. 3, pp. 32–57, 1973.
- [20] A. Elazab, C. Wang, F. Jia, J. Wu, G. Li, and Q. Hu, "Segmentation of brain tissues from magnetic resonance images using adaptively regularized kernel-based fuzzy-means clustering," *Comput. Math. Methods Med.*, vol. 2015, pp. 1–12, Nov. 2015. doi: [10.1155/2015/485495](https://doi.org/10.1155/2015/485495).
- [21] J. Fan, D. K. Y. Yau, A. K. Elmagarmid, and W. G. Aref, "Automatic image segmentation by integrating color-edge extraction and seeded region growing," *IEEE Trans. Image Process.*, vol. 10, no. 10, pp. 1454–1466, Oct. 2001.
- [22] R. R. Gharieb, G. Gendy, A. Abdelfattah, and H. Selim, "Adaptive local data and membership based KL divergence incorporating C-means algorithm for fuzzy image segmentation," *Appl. Soft Comput.*, vol. 59, pp. 143–152, Oct. 2017.
- [23] M. Girolami, "Mercer kernel-based clustering in feature space," *IEEE Trans. Neural Netw.*, vol. 13, no. 3, pp. 780–784, May 2002.
- [24] M. Gong, Y. Liang, J. Shi, W. Ma, and J. Ma, "Fuzzy C-means clustering with local information and kernel metric for image segmentation," *IEEE Trans. Image Process.*, vol. 22, no. 2, pp. 573–584, Feb. 2013.
- [25] D. Graves and W. Pedrycz, "Kernel-based fuzzy clustering and fuzzy clustering: A comparative experimental study," *Fuzzy Sets Syst.*, vol. 161, no. 4, pp. 522–543, Feb. 2010.
- [26] R. Krishnapuram and J. M. Keller, "A probabilistic approach to clustering," *IEEE Trans. Fuzzy Syst.*, vol. 1, no. 2, pp. 98–110, May 1993.
- [27] R. Krishnapuram and J. M. Keller, "The probabilistic C-means algorithm: Insights and recommendations," *IEEE Trans. Fuzzy Syst.*, vol. 4, no. 3, pp. 385–393, Aug. 1996.
- [28] K.-P. Lin, "A novel evolutionary kernel intuitionistic fuzzy C-means clustering algorithm," *IEEE Trans. Fuzzy Syst.*, vol. 22, no. 5, pp. 1074–1087, Oct. 2014.
- [29] P.-L. Lin, P.-W. Huang, C. H. Kuo, and Y. H. Lai, "A size-insensitive integrity-based fuzzy C-means method for data clustering," *Pattern Recognit.*, vol. 47, no. 5, pp. 2041–2056, May 2014.
- [30] Z. Liu, S. Xu, Y. Zhang, and C. L. P. Chen, "A multiple-feature and multiple-kernel scene segmentation algorithm for humanoid robot," *IEEE Trans. Cybern.*, vol. 44, no. 11, pp. 2232–2240, Nov. 2014.
- [31] Y. Lv, Y. Chen, X. Zhang, Y. Duan, and N. Li, "Social media based transportation research: the state of the work and the networking," *IEEE/CAA J. Autom. Sinica*, vol. 4, no. 1, pp. 19–26, Jan. 2017.
- [32] J. Ma, D. Tian, M. Gong, and L. Jiao, "Fuzzy clustering with non-local information for image segmentation," *Int. J. Mach. Learn. Cybern.*, vol. 5, no. 6, pp. 845–859, Dec. 2014.
- [33] J. C. Mason and D. C. Handscomb, *Chebyshev Polynomials*. London, U.K.: Chapman and Hall, 2003.
- [34] J. Niyobuhungiro and E. Setterqvist, "A new reiterative algorithm for the Rudin–Osher–Fatemi denoising model on the graph," in *Proc. 2nd Int. Conf. Intell. Syst. Image Process.*, Sep. 2014, pp. 81–88.
- [35] J. C. Pichel, D. E. Singh, and F. F. Rivera, "Image segmentation based on merging of sub-optimal segmentations," *Pattern Recognit. Lett.*, vol. 27, no. 10, pp. 1105–1116, Jul. 2006.
- [36] A. Ron and Z. Shen, "Affine systems in  $L_2(\mathbb{R}^d)$ : The analysis of the analysis operator," *J. Funct. Anal.*, vol. 148, no. 2, pp. 408–447, Aug. 1997.
- [37] L. Rudin, S. Osher, and E. Fatemi, "Nonlinear total variation based noise removal algorithms," *Physica D Nonlin. Phenom.*, vol. 60, no. 1–4, pp. 259–268, Nov. 1992.
- [38] H. Shen, J. Yang, S. Wang, and X. Liu, "Attribute weighted mercer kernel based fuzzy clustering algorithm for general non-spherical datasets," *Soft Comput.*, vol. 10, no. 11, pp. 1061–1073, Sep. 2006.
- [39] A. Singer, "From graph to manifold Laplacian: The convergence rate," *Appl. Comput. Harmon. Anal.*, vol. 21, no. 1, pp. 128–134, Jul. 2006.
- [40] L. Szilagyi, Z. Benyo, S. Szilagyi, and H. Adam, "MR brain image segmentation using an enhanced fuzzy C-means algorithm," in *Proc. IEEE 25th Annu. Int. Conf. EMBS*, Sep. 2003, pp. 724–726.
- [41] K. S. Tan and N. A. M. Isa, "Color image segmentation using histogram thresholding—Fuzzy C-means hybrid approach," *Pattern Recognit.*, vol. 44, no. 1, pp. 1–15, Jan. 2011.
- [42] H. Wang, Y. Jin, and J. O. Jansen, "Data-driven surrogate-assisted multiobjective evolutionary optimization of a trauma system," *IEEE Trans. Evol. Comput.*, vol. 20, no. 6, pp. 939–952, Dec. 2016.
- [43] C. Wang and J. Yang, "Poisson noise removal of images on graphs using tight wavelet frames," *Vis. Comput.*, vol. 34, no. 10, pp. 1357–1369, Oct. 2018.
- [44] T. Xu, L. Jiao, and W. J. Emery, "SAR image content retrieval based on fuzzy similarity and relevance feedback," *IEEE J. Sel. Topics Appl. Earth Observ. Remote Sens.*, vol. 10, no. 5, pp. 1824–1842, May 2017.
- [45] J. Yang and C. Wang, "A wavelet frame approach for removal of mixed Gaussian and impulse noise on surfaces," *Inverse Problem Imag.*, vol. 11, no. 5, pp. 783–798, Oct. 2017.
- [46] J. Yang, G. Zhu, D. Tong, L. Lu, and Z. Shen, "B-spline tight frame based force matching method," *J. Comput. Phys.*, vol. 362, no. 1, pp. 208–219, Jun. 2018.
- [47] X. Zhu, W. Pedrycz, and Z. W. Li, "Fuzzy clustering with nonlinearly transformed data," *Appl. Soft Comput.*, vol. 61, pp. 364–376, Dec. 2017.



**Cong Wang** received the B.S. degree in automation from the College of Internet of Things Engineering, Hohai University (Changzhou Campus), Changzhou, China, in 2014 and the M.S. degree in mathematics from the Department of mathematics, Hohai University, Nanjing, China, in 2017. He is currently pursuing the Ph.D. degree in mechatronic engineering with Xidian University, Xi'an, China.

His current research interests include wavelet analysis and its applications, granular computing, and pattern recognition and image processing.

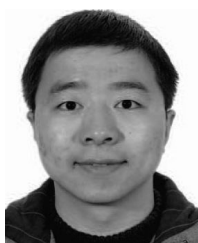


**Witold Pedrycz** (M'88–SM'90–F'99) received the M.Sc., Ph.D., and D.Sci., degrees from the Silesian University of Technology, Gliwice, Poland.

He is a Professor and the Canada Research Chair of computational intelligence with the Department of Electrical and Computer Engineering, University of Alberta, Edmonton, AB, Canada. He is currently with the School of Electro-Mechanical Engineering, Xidian University, Xi'an, China, and the Faculty of Engineering, King Abdulaziz University, Jeddah, Saudi Arabia. He is also with the Systems Research

Institute, Polish Academy of Sciences, Warsaw, Poland, where he is a Foreign Member. He has authored 15 research monographs covering various aspects of computational intelligence, data mining, and software engineering. His current research interests include computational intelligence, fuzzy modeling, and granular computing, knowledge discovery and data mining, fuzzy control, pattern recognition, knowledge-based neural networks, relational computing, and software engineering. He has published numerous papers in the above areas.

Dr. Pedrycz was a recipient of the IEEE Canada Computer Engineering Medal, the Cajastur Prize for Soft Computing from the European Centre for Soft Computing, the Killam Prize, and the Fuzzy Pioneer Award from the IEEE Computational Intelligence Society. He is intensively involved in editorial activities. He is the Editor-in-Chief of *Information Sciences*, *WIREs Data Mining and Knowledge Discovery* (Wiley), and the *International Journal of Granular Computing* (Springer). He currently serves as a member of a number of editorial boards of other international journals. He is a fellow of the Royal Society of Canada.



**JianBin Yang** received the B.S. degree in applied mathematics from Yangzhou University, Yangzhou, China, in 2005 and the Ph.D. degree in applied mathematics from Zhejiang University, Hangzhou, China, in 2010.

He was a Research Fellow with the Department of Mathematics, National University of Singapore, Singapore, from 2013 to 2014. He is currently an Associate Professor of mathematics with Hohai University, Nanjing, China. His current research interests include image processing, and wavelet analysis and its applications.



**MengChu Zhou** (S'88–M'90–SM'93–F'03) received the B.S. degree in control engineering from the Nanjing University of Science and Technology, Nanjing, China, in 1983, the M.S. degree in automatic control from the Beijing Institute of Technology, Beijing, China, in 1986, and the Ph.D. degree in computer and systems engineering from Rensselaer Polytechnic Institute, Troy, NY, USA, in 1990.

In 1990, he joined the New Jersey Institute of Technology, Newark, NJ, USA, where he is currently a Distinguished Professor of electrical and computer engineering. He is also currently with the Institute of Systems Engineering, Macau University of Science and Technology, Macau, China. He has over 800 publications, including 12 books, over 460 journal papers (over 360 in IEEE TRANSACTIONS), 12 patents, and 29 book chapters. His current research interests include Petri nets, intelligent automation, Internet of Things, big data, Web services, and intelligent transportation.

Dr. Zhou was a recipient of the Humboldt Research Award for U.S. Senior Scientists from Alexander von Humboldt Foundation, the Franklin V. Taylor Memorial Award, and the Norbert Wiener Award from IEEE Systems, Man and Cybernetics Society for which he serves as the VP for conferences and meetings. He is the Founding Editor of IEEE Press Book Series on Systems Science and Engineering and the Editor-in-Chief of the IEEE/CAA JOURNAL OF AUTOMATICA SINICA. He is a Life Member of the Chinese Association for Science and Technology, USA, and served as its President in 1999. He is a fellow of the International Federation of Automatic Control, the American Association for the Advancement of Science, and the Chinese Association of Automation.



**ZhiWu Li** (M'06–SM'07–F'16) received the B.S. degree in mechanical engineering, the M.S. degree in automatic control, and the Ph.D. degree in manufacturing engineering from Xidian University, Xi'an, China, in 1989, 1992, and 1995, respectively.

He joined Xidian University in 1992. He is currently with the Institute of Systems Engineering, Macau University of Science and Technology, Macau, China. He was a Visiting Professor with the University of Toronto, Toronto, ON, Canada; the Technion-Israel Institute of Technology, Haifa, Israel; the Martin-Luther University of Halle-Wittenberg, Halle, Germany; the Conservatoire National des Arts et Métiers, Paris, France; and Meliksah Universitesi, Kayseri, Turkey. His current research interests include Petri net theory and application, supervisory control of discrete-event systems, workflow modeling and analysis, system reconfiguration, game theory, and data and process mining.

Dr. Li was a recipient of the Alexander von Humboldt Research Grant and the Alexander von Humboldt Foundation, Germany. He is listed in Marquis Who's Who in the World, 27th Edition, 2010. He serves as a Frequent Reviewer of over 90 international journals, including *Automatica* and a number of the IEEE TRANSACTIONS as well as many international conferences. He is the Founding Chair of Xi'an Chapter of IEEE Systems, Man, and Cybernetics Society. He was a member of Discrete-Event Systems Technical Committee of the IEEE Systems, Man, and Cybernetics Society and IFAC Technical Committee on Discrete-Event and Hybrid Systems from 2011 to 2014.